IEEE Access
Multidisciplinary | Rapid Review | Open Access Journal

Received 12 February 2023, accepted 27 February 2023, date of publication 16 March 2023, date of current version 23 March 2023.

Digital Object Identifier 10.1109/ACCESS.2023.3258401

RESEARCH ARTICLE

The Omnirotor Platform: A Versatile, Multi-Modal, Coaxial, All-Terrain Vehicle

JOAO BUZZATTO, (Graduate Student Member, IEEE), AND MINAS LIAROKAPIS, (Senior Member, IEEE)
New Dexterity Research Group, Department of Mechanical and Mechatronics Engineering, The University of Auckland, Auckland, New Zealand
Corresponding author: Joao Buzzatto (jsan819@aucklanduni.ac.nz)

ABSTRACT Mobile and aerial robots offer many potential applications, including warehouse logistics, surveillance, cinematography, and search and rescue. However, most such robots are task-specific and generally lack the versatility to tackle multiple scenarios, terrains, and unstructured, dynamic environments. This paper presents the Omnirotor platform, a versatile, multi-modal, coaxial, tilt-rotor, all-terrain vehicle that combines an Unmanned Aerial Vehicle (UAV) and an Unmanned Ground Vehicle (UGV) into a hybrid, all-terrain vehicle. The Omnirotor has two locomotion modes of operation (aerial and ground vehicle) and five operational configurations, as it can fly both in the Normal and Inverted configurations and drive on the ground in the Normal and Inverted configurations. It can also recover from any non-operational state to its Normal, upside-down configuration. Moreover, in addition to the locomotion modes, the continuous omnidirectional thrust vectoring enables the Omnirotor platform to perform complex manipulation of objects. This work introduces the concept and discusses in detail the design, development, and experimental validation of the Omnirotor platform. In particular, it discusses the modeling and control schemes required by the different operation modes and configurations. It experimentally validates the platform's capabilities with experiments focusing on traversing challenging environments and unstructured, uneven terrains (e.g., a public park). Finally, the platform's ground, pushing-based manipulation capabilities are demonstrated through the execution of a puzzle-solving experiment where the solved puzzle serves as a landing platform for the all-terrain vehicle. The versatility of the Omnirotor offers exciting prospects for use in challenging search-and-rescue scenarios, surveillance, and aerial and ground manipulation applications.

INDEX TERMS Robotics and automation, autonomous aerial vehicles, rescue robots, robot control, manipulators, mobile robots.

I. INTRODUCTION

Unmanned Aerial Vehicles (UAVs) and Unmanned Ground vehicles (UGV) are employed in many industries, including cinematographic, inspection, entertainment, surveillance, search-and-rescue, and security. In the interest of improving the current capabilities and expanding the use of UAVs and UGVs for other applications, researchers are exploring new design paradigms and concepts. Recent research efforts include developing UAVs capable of efficient physical interaction with dynamic environments to enable the execution of complex tasks such as dexterous manipulation [1], [2], and the development of multi-modal or hybrid vehicles that exhibit the characteristics of both ground and aerial vehicles [3], [4].

In the related literature on hybrid UAV/UGV, only a few proposed hybrid concepts are collision resilient and capable of recovering and returning to regular operation after a crash. This lack of resilience significantly decreases their suitability to work in unstructured and dynamic environments. Furthermore, none of these works demonstrated that their design is capable of interacting with the environment or performing manipulation tasks. Manipulation capabilities are instrumental when navigating, for example, cluttered and unstructured environments such as the inside of a building after an earthquake. In such cases, pushing chairs, boxes, and other objects

The associate editor coordinating the review of this manuscript and approving it for publication was Gerardo Flores.

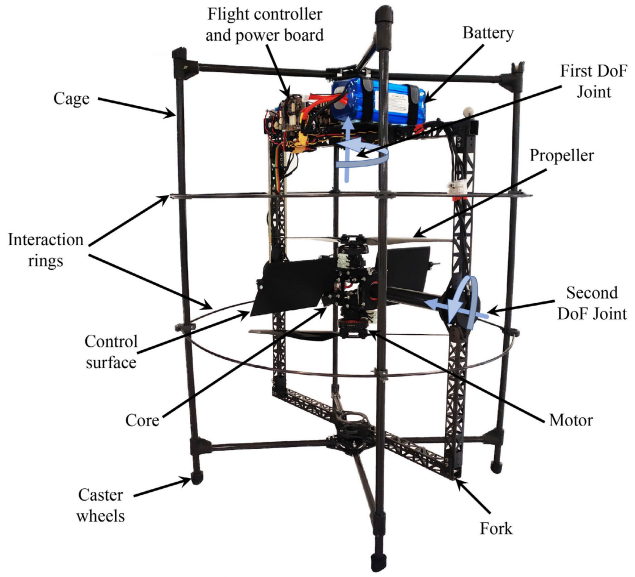

FIGURE 1. The New Dexterity Omnirotor platform, a hybrid, multi-modal, all-terrain robotic vehicle with continuous omnidirectional thrust vectoring capabilities. The concept has two different modes of operation (ground and aerial vehicle), four operation configurations, and a process. The four configurations are flight in both the Inverted and Normal pose, ground operation in both the Inverted and Normal pose, and the process is the recovery action that can bring the vehicle from any non-operational state to its Normal ground pose. The concept achieves continuous omnidirectional thrust vectoring employing a rotor-on-gimbal mechanism [5], [6]. In particular, a coaxial rotor is placed inside a gimbal mechanism that has two perpendicular rotating actuated Degrees of Freedom (DoF), represented by the blue arrows. The prototype comprises three main bodies: i) the Core, which houses the mechanism enabling the rotor-on-gimbal; ii) the Fork, where the flight controller, battery, and other electronics are mounted; and iii) the Cage, which protects the other components of the vehicle and enables safe interaction with the environment. Furthermore, the upper and lower flat sides of the cage have each four omnidirectional, holonomic caster wheels that allow the vehicle to drive on the ground in both configurations.

out of the way can enable the vehicle to transverse environments a regular hybrid vehicle would not be able to. In this work, we present the Omnirotor platform, which is, to the best of the authors' knowledge, the first hybrid UAV/UGV vehicle that is collision resilient, capable of recovery, and demonstrates it can interact with the environment, performing complex manipulation tasks.

The Omnirotor platform [5], [6] is a coaxial [7], ultra-versatile, multi-modal, hybrid, tilt-rotor UAV/UGV vehicle, and the first concept to demonstrate the capability of continuous omnidirectional thrust vectoring, meaning it can apply its full thrust in any direction in a continuous, unconstrained manner. This paper presents an improved prototype version of the concept (Fig. 1) that utilizes a novel approach to create the rotor-on-gimbal mechanism. Here we demonstrate the capabilities of both the aerial and ground vehicle operation modes and take advantage of its omnidirectional thrust vectoring capability to demonstrate other abilities that improve on what has been demonstrated so far by other concepts in the literature. Namely, such abilities are its four different operating configurations, which include flying in two configurations (Normal and Inverted), driving on the ground also in two configurations (Normal and Inverted), and lastly, the recovery process, which restores the vehicle to its Normal ground operational configuration after crashing and landing on its side or in any non-operational state. Additionally, the Omnirotor can also perform ground push-based manipulation of objects in its Normal and Inverted pose. Equivalently, we also demonstrate that the vehicle can takeoff even from inclined surfaces and uneven ground. This combination of features makes the Omnirotor concept ideal for search-and-rescue applications, where fast response and the continuous exploration of unstructured environments demand versatility, resilience, and high autonomy.

The rest of the paper is organized as follows: Section II presents some related work in the field, section III presents the platform's design, Section IV describes the modeling and control, Section V presents experimental results and discussions, while Section VI concludes the paper.

II. RELATED WORK

Manipulation is one of the most demanding classes of tasks for a UAV, and turning aerial vehicles into manipulators is a challenge in terms of both hardware and software. Aerial manipulator platforms typically consist of the following two subsystems: i) the aerial vehicle and ii) the manipulation system that is used for interaction with the environment [8], [9]. Regarding the vehicle type, aerial manipulators typically belong to one of the following classes: i) helicopters [2], [10], ii) unidirectional multirotors, such as quadrotors [1] and hexacopters [11], iii) ducted-fan vehicles [12], iv) fixed-wing designs [13], and v) hybrid designs [14]. Although unidirectional UAVs are very useful for many applications, they are not well suited for aerial manipulation tasks since their underactuated nature limits their dexterity. [15], [16], [17]. Researchers have tried to overcome the drawbacks of unidirectional multirotor UAVs by proposing novel designs that employ fully actuated or even overactuated concepts. The available literature suggests two approaches in this direction: i) concepts with fixed tilted rotors [18], and ii) vehicles powered by active tilting rotors [19], [20], [21], [22]. Despite being lighter, fixed tilted rotor vehicles display limited versatility, as they usually operate with a single stable orientation and cannot exert significant forces in relation to their weight on the surrounding environment. Alternatively, active rotor-tilting UAV concepts have such interaction capabilities but have the drawback of being heavier, bulkier, and more mechanically complex.

One of the most significant limitations of aerial vehicles is their operation time, which is generally quite limited. On the other hand, ground vehicles are very energy efficient and can operate for extended periods. Vehicles with both ground and aerial locomotion capabilities are appealing precisely because of the extended autonomy the ground mode can provide. Such hybrid capabilities are achieved with many approaches, with most falling into the following: i) passive

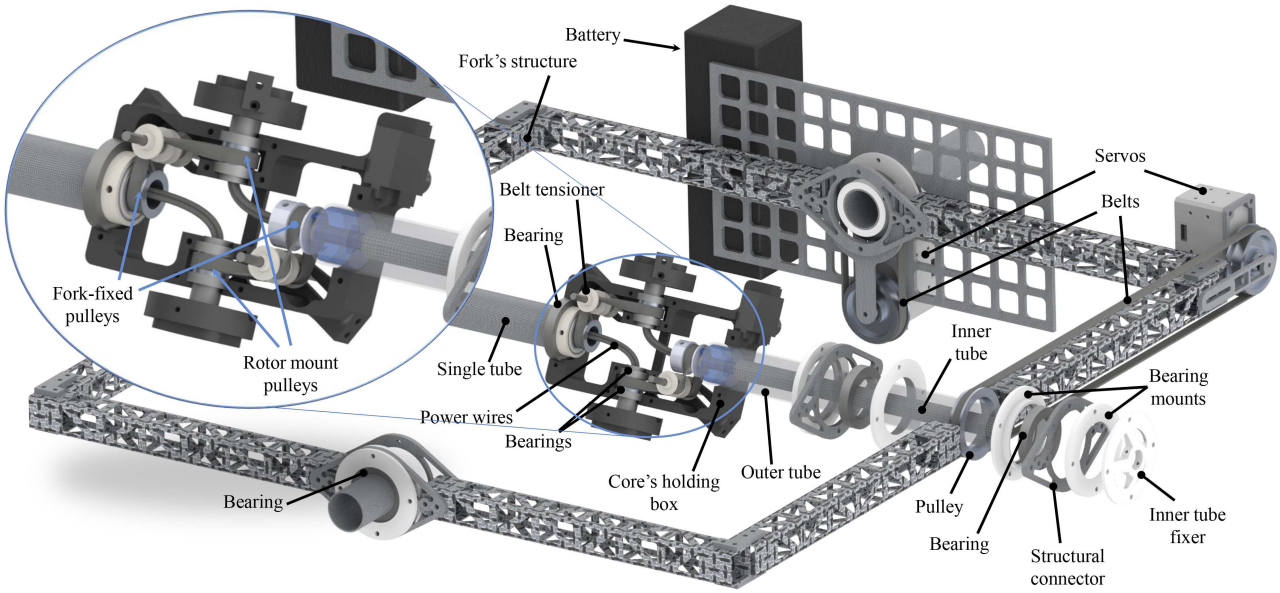

FIGURE 2. Annotated exploded view of the design focusing on the new rotor-on-gimbal mechanism encompassing the Core and Fork module bodies. All the motions of the gimbal DoF are facilitated with timing belts and pulleys. Both servo motors are mounted on the Fork structure. For the first DoF, the output pulley is connected to a tube fixed on the Cage. The second DoF has the servo mounted at the same level as the battery, and it uses a large belt to drive the output pulley connected to a tube fixed to the Core's holding box. Inside such a tube is a smaller tube that is instead fixed to the Fork. This and another pulley fixed to the Fork have the motor wires running through them and connecting to the speed controllers and battery. These Fork-fixed pulleys are connected with a 90° bent transmission belt to the rotor-fixed pulleys. The pulleys sharing the same belt do not share the same wires, ensuring that untangling of the wires will be accomplished.

wheels [5], [6], [23], [24], [25], [26], ii) passive rotating cage [3], [27], [28], [29], iii) active wheels [4], [30], [31], [32], [33], or active legs [34], [35]. The passive rotating structures are likely the most lightweight and simple solution to turn an aerial vehicle into a hybrid one. However, since they rely on the vehicle's propulsion system for ground locomotion, operational precision in this mode is inferior compared to active wheels. The latter sacrifices payload capacity by adding the weight of extra actuators for actively driving on the ground using the wheels. Finally, the legged approach forgoes even more payload and simplicity of design for the ability to cross rough and uneven terrain in ground mode.

III. DESIGN

This section describes the fundamental concepts behind the design of the Omnirotor platform presented in this work. It also details how these design concepts were implemented in the prototype. Subsection A elaborates on the rotor-on-gimbal mechanism, which enables continuous omnidirectional thrust vectoring. Subsection B, explains how additional controls are needed in the rotor-on-gimbal mechanism and how adding control surfaces between the coaxial rotors is a viable solution. Finally, subsection C details the prototype building materials and components.

A. THE ROTOR-ON-GIMBAL MECHANISM

Considering the goal of designing a rotor module with continuous omnidirectional thrust vectoring, the most straightforward approach is to mount the rotors on a structure that rotates around two perpendicular axes. This type of mechanism is called a gimbal, and it is predominantly used in camera systems. However, wiring is the immediate constraint that stems from such a method. Every active rotor tilting mechanism is restricted in its ability to turn by the amount its wire connections can coil around the rotating axis. Slip-rings, which are effectively rotational electric connections, are the conventional solution for these wiring constraints. This is also popular in gimbal camera stabilization systems. However, brushless electric motors used in propulsion systems demand massive amounts of electric current, resulting in large and heavy slip-rings. This increased weight is undesirable because it significantly reduces the vehicle's flight time and payload capacity.

In previous works, the authors proposed the solution of placing the battery together with the rotors, leaving only wire connections with low current passing through the slip-rings to the control electronics [5], [6]. However, such a solution suffers from some problems. First, since the battery is cased tightly between the coaxial rotors and the structure, battery replacement is cumbersome and not flexible regarding battery geometry and footprint. Second, given that the battery represents about a third of the vehicle's weight, placing it near the rotors brings the vehicle's Center of Gravity (CG) closer to them, reducing the attitude control authority of the rotors and control surfaces. Such problems motivated the development of a new mechanism inside the gimbal that retains the omnidirectionality and the unconstrained rotation capability while allowing the battery to be placed away from the rotors, increasing the CG's distance from the actuators and therefore improving attitude control authority.

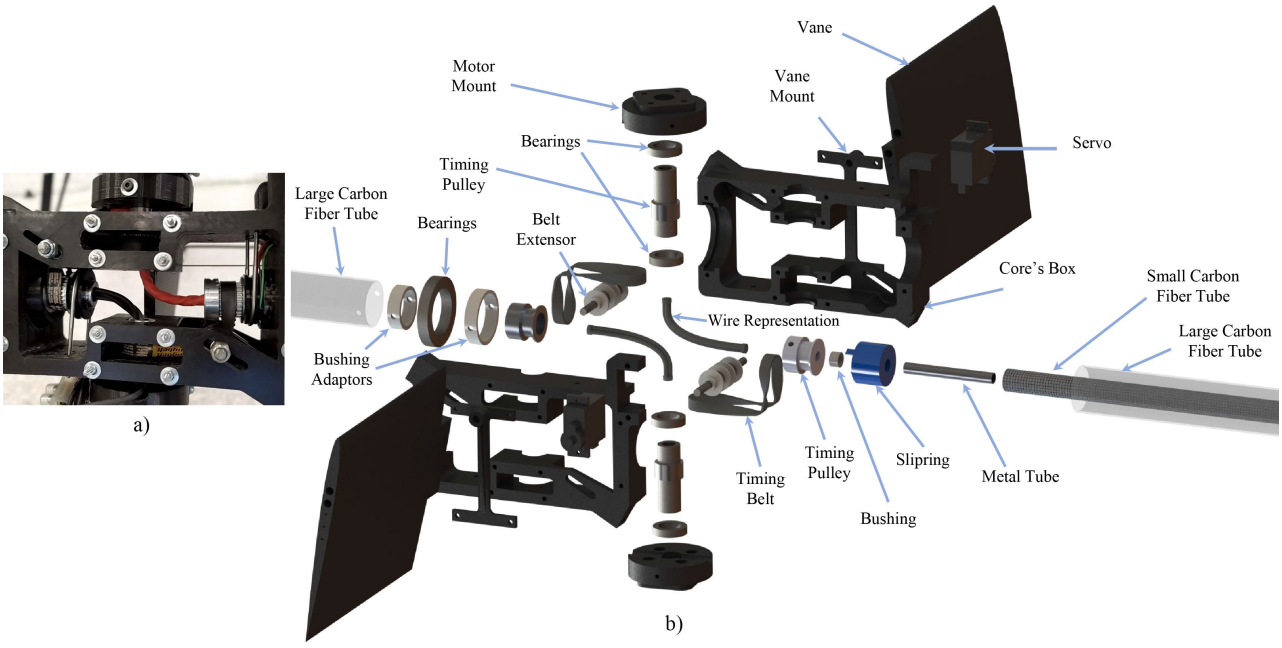

FIGURE 3. Subfigure a), presents a screenshot of the video showing the mechanism developed for the rotor-on-gimbal concept. The video provides a better understanding of the mechanism, and readers are highly recommended to watch it. The figure displays a close-up view of the Core mechanism as having a fixed frame to the Core holding box. As the Core link rotates, from this point of view, the Fork fixed pulleys (horizontally aligned pulleys) appear to rotate, driving the rotor-fixed pulleys (vertically aligned pulleys) connected to them to rotate in the same direction. By passing the wires through the pulleys not connected by belts, which rotate opposite to the direction of the belt-connected pulleys, the mechanism ensures that the wires never get twisted. Subfigure b) shows the exploded view of the mechanism with a detailed annotation.

Such a new mechanism is illustrated in Fig. 2, and it is part of the vehicle's structure we call 'Core.' It consists of two pairs of pulleys, one pair for each rotor. Each pair has its rotating axes perpendicular to each other. As in Fig. 3, the pulleys attached to the rotor mount are free to rotate. The other pulleys are fixed with respect to the other primary vehicle's structure that we call the 'Fork' but can rotate with respect to the Core's holding box. All pulleys have a hole where the wires from the motors pass through. The belts and wires are arranged so that each pair of pulleys sharing the same wires do not share the same belt. The result is that the wire-sharing pair of pulleys counter-rotate with each other. This way, while the Core's box rotates with respect to the stationary pulleys, twisting the wires, the rotating pulleys turn in the opposite direction, untwisting the wires. For a better comprehension of the working principle of the proposed mechanism, please refer to Figure 3 and to the video that can be found in subsection V-F.

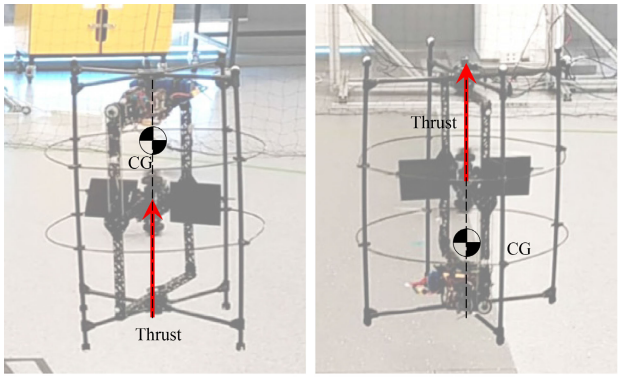

FIGURE 4. Illustration of the two possible hovering stable points for the all-terrain vehicle concept. The CG of the craft must be in line with the rotors' thrust for it to hover stably. This happens when the CG is either above the rotors (Inverted equilibrium) or below them (Normal equilibrium). For the current design, such equilibrium points coincide with the gimbal kinematic singularity, which is aligned with the axis of the first DoF.

B. CONTROL SURFACES IN BETWEEN COAXIAL ROTORS

The disadvantage of the gimbal mechanism is its singularity points. These are the locations in its workspace where, when using inverse kinematics to follow a path, small changes in the direction that the platform is pointed at produce significant joint motions (mainly for the first DoF). As a result, while operating close to such singularity points, the rotor-on-gimbal mechanism cannot swiftly make minor force corrections without disturbing the system. Unfortunately, in the proposed all-terrain vehicle with a single rotor-on-gimbal module [5], the system's CG is always aligned with the kinematic singularity for both of its stable configurations (see Fig. 4).

This problem is solved by adding control surfaces downstream to the propellers, arranged perpendicularly to the second DoF. Even when operating at the gimbal's singularity points, this addition provides sufficient control authority in

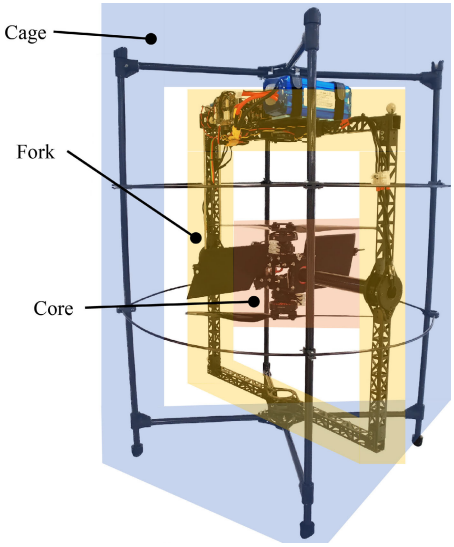

FIGURE 5. Illustration highlighting the main bodies composing the Omnirotor platform. These main bodies are i) the Cage, which protects the other components of the vehicle and is the component where the caster wheels are attached; ii) the Fork, which bridges the Core and the Cage, where the flight controller and most other electronics are attached, and finally iii) the Core, which houses the wire untwisting mechanism, the control surfaces, and the rotors.

all directions, eliminating the need for sophisticated control algorithms for compensation, such as online weight optimizations. However, given the limited space for such a design change and the desire to keep the rotor-on-gimbal design as small as possible, it was decided to place the control surfaces between the coaxial rotors (Fig. 1). Despite the significant added complexity to the system, particularly in the aerodynamic sense, this solution approach is lightweight, simple to implement, inexpensive, and proved to be effective.

C. PROTOTYPE AND HARDWARE

This subsection details the prototype's components, building materials, and manufacturing. Subsection I) focuses on the Outer Cage protecting the Omnirotor, subsection II) describes the Fork body, while subsection III) focuses on the Core subassembly. Each of these bodies is illustrated in Fig. 5.

The current prototype presents some noticeable differences compared to its predecessor, particularly in the areas of wiring management and electronic component arrangement. The most notable difference is its size, as the new prototype is approximately two times larger. The decision to increase the size of the concept served a dual purpose. Firstly, it allowed for an evaluation of the scalability of the design, and secondly, it aimed to improve the vehicle's overall efficiency, flight time, and payload capacity. This is because larger rotors are known to be more efficient than smaller ones, and thus, increasing the size of the prototype was expected to result in a higher level of efficiency and greater payload capacity. Moreover, the larger payload capacity enables using a broader range of components, such as servo motors, cameras, and grippers, reducing the restrictions faced during prototyping. It is worth noting that control surfaces are used in aircrafts of all sizes. However, it must be acknowledged that scaling up the prototype also comes with added manufacturing costs and increased time, as well as more challenging testing conditions.

Additionally, the authors anticipate that the larger versions may face difficulties navigating indoor environments. Despite these trade-offs, the authors believe that the current form factor of the prototype strikes a balance between autonomy, payload capacity, cost, and applicability to various scenarios. Despite these changes, the software system remains largely the same, relying on PX4 as its central component. However, the firmware has undergone additional modifications to enhance its ability to support various operational configurations. The code can be found at the following URL:

https://github.com/newdexterity/OmniRotor-Firmware

1) OUTER CAGE

The vehicle structure is mainly built out of carbon fiber profiles and sheets to give the vehicle rigidity while being lightweight. The outer cage uses 12 mm carbon fiber tubes joined together with 90° custom-made connectors. These connectors are fabricated with the process known as forged carbon fiber, where an amorphous mix of epoxy resin and short strands of carbon fiber is molded into a complex 3D shape. At the connection points to the fork body, the cage's tubes are attached using water-jet cut 3 mm carbon fiber sheets and 3D printed PLA adapters. Additionally, two horizontal rings are added to the cage to provide a compliant, lightweight structure that serves both the purpose of protection and is also used as a tool to interact with the environment. The rings are made of straight, 4 mm pull-threaded carbon fiber rods bent into shape and fixed with SLS Nylon 3D printed connectors. Finally, the top and bottom ends of the cage accommodate 1-inch in diameter Pololu plastic ball caster wheels, allowing the vehicle to drive on the ground when in ground mode.

2) FORK

The Fork structure contains many of the main components of the design, including the Pixhawk 4 flight controller, the two T-Motor AIR 40A 6S speed controllers, the 6000 mAh LiPo battery, and the two Dynamixel XM430-W350-T servo motors that actuate the two active DoF of the gimbal. In fact, since the flight controller is mounted on it, the Fork body can be considered as the whole vehicle when flying, as explained in Section IV. The structures forming the rectangle shape of the Fork consist of 20 × 20 mm carbon fiber square tubes. A truss-like pattern was cut into them for weight optimization using the water-jet cutter. Both connection points to the Cage are supported with bearings fit with 25 mm diameter tubes, while the tubes are fixed with respect to the Cage. The motion of the servo motors is transmitted with timing belts and pulleys. The servo for the second DoF is placed at the same level as all other electronics to keep the CG as high and far as

TABLE 1. Table with the weight distribution of the Omnirotor prototype.

Component	Cage	Caster Wheel	All Caster Wheels	Fork + Core	Total
Weight [g]	580	19	152	3120	3700
% of Total	16	0.51	4.1	84	

possible from the rotors, requiring a long belt to actuate the Core body.

3) CORE

A 3D printed PLA-based split box joints all Core body components. The rotors (T-Motor MN5006 KV450 motor and 16.2 inches propellers) are mounted on a 3D printed PLA part attached to a steel tube that also features a timing pulley. The belts need strong tensioning to avoid slipping, and the resultant force on the pulleys needs to be countered to prevent failure. The pulleys connected to motors have a pair of bearings, one on each side of the belt. The Fork-fixed pulleys use "U" shaped steel rods and bearings to compensate for the belt forces. These last structures are omitted in the exploded view of Fig. 2 to avoid cluttering the image. In that figure, the left side of the box also has 9 g micro servos used to actuate the control surfaces placed in between the coaxial rotors. This box side also has a hole-through slip-ring to power and control the micro servos. The slip-ring is slotted inside a 25 mm tube, and a smaller diameter tube passes through the slip-ring accommodating the wires that power one of the rotors. In turn, this smaller tube is fixed to the Fork body, while the larger tube is fixed to the Core's box and transmits the rotation from the servo motor and pulley system (Fig. 3 b)). The right side of the box is attached to a bearing fixed to a tube that is fixed to the Fork. The box rotates freely with respect to the tube.

The control surfaces, or vanes, are 3D-printed PLA NACA 0006 airfoil profiles with 115 mm chord length and 150 mm span. The vanes hinge about 4 mm carbon fiber rods, which are press-fitted into 3D-printed PLA holders assembled onto the Core's box. The servo horns and the vanes are connected by 0.8 mm steel rods, and together they form a parallel four-bar linkage which guarantees that the vane angle is equal to the servo angle.

Overall, the vehicle weighs 3.7 kg, has a flight time of about 8 minutes, and has a payload capacity of 0.6 kg with a 6000 mAh battery, when flying in the Inverted configuration. While on ground mode, the platform demands much less energy and can operate for about 40 to 50 minutes, depending on the roughness and inclination of the terrain. A summary of the vehicle's weight distribution is presented in Table 1, while some important characteristics are summarized in Table 2.

IV. MODELING AND BASIC CONTROL

This section presents the system modeling and the control common to all flight configurations. Subsection A presents the free-floating model for the vehicle, and subsection B, introduces the position and attitude control used for all flight configurations, which is the standard from PX4, and the curious reader can find further information such as proof of stability and performance characteristics in [36] and [37]. Finally, subsection C, explains how the control surfaces are controlled.

TABLE 2. Table summarizing the characteristics of the Omnirotor.

Characteristic	Value
Total Weight	3.7 kg
Maximum Thrust	46 N
Maximum Payload	0.6 kg
Flight Time Inverted	8 minutes
Flight Time - Normal	5 minutes
Ground Drive Time	40-50 minutes

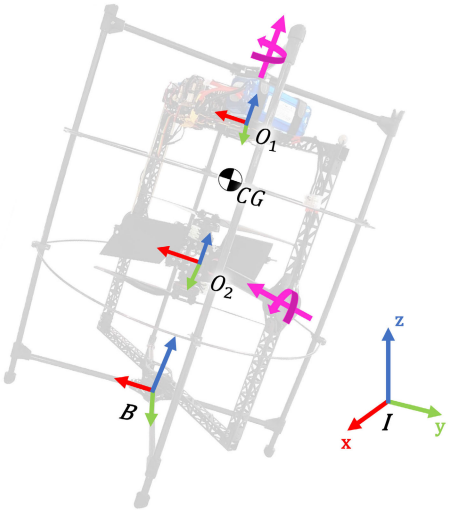

FIGURE 6. The reference frames used for modeling and inverse kinematics of the Omnirotor all-terrain platform are depicted in this diagram. The red, green, and blue arrows represent the reference frames' *x*, *y*, and *z* axis, respectively. Frame *I* is the inertial reference frame, frame *B* is the frame attached to the vehicle's Cage, frame O_1 is attached to the Fork body, and frame O_2 is attached to the Fork body. The first DoF joint that connects the Cage to the Fork body is in the direction of $\hat{z}_b$ and $\hat{z}_1$, while the second DoF joint is in the direction of $\hat{x}_1$ and $\hat{x}_2$. The pink arrows represent the joints.

A. MODELING

Consider first the inertial reference frame denoted by $I = \{\hat{x}, \hat{y}, \hat{z}\}$. $B = \{\hat{x}_b, \hat{y}_b, \hat{z}_b\}$ is the frame rigidly attached to the vehicles cage. Additionally, $O_1 = \{\hat{x}_1, \hat{y}_1, \hat{z}_1\}$ is attached to the Fork, and $O_2 = \{\hat{x}_2, \hat{y}_2, \hat{z}_2\}$ is attached to the core, which contains the rotors, as shown in Fig. 6. However, for simplicity, the Omnirotor is considered here as a single rigid body, with the rotor's thrust, $T \in \mathbb{R}^3$, applied at the origin of O_2. Consequently, the dynamic effects caused by the movement of the gimbal's links are considered to be negligible.

This consideration keeps the equations of motion simple and suits well for control purposes given the underactuated

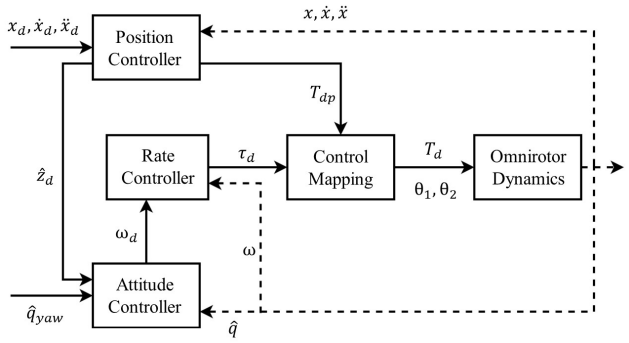

FIGURE 7. A control block diagram illustrating the control scheme used on the Omnirotor. It consists of a position controller that seats at the highest level, which then passes information to both the attitude controller and the control mapping blocks. The second highest level is the attitude controller, which provides information to the rate controller, which, together with the control mapping block, forms the lower level part of the controller. In the control scheme, the higher the block level, or the outer it seats in the scheme, the lower its operating frequency. Control blocks in the center of the diagram are more fundamental to the system's stability and require high operating frequencies. In this representation, the dashed lines represent measurements from the system.

nature of the system. Under such assumptions, using the Newton-Euler formalism, the equations of motion for our system are

$$m\ddot{\boldsymbol{x}} = \boldsymbol{T} - m\,g\,\hat{\boldsymbol{z}}, \tag{1}$$

$$J\,\dot{\boldsymbol{\omega}} + \boldsymbol{\omega} \times J\,\boldsymbol{\omega} = \boldsymbol{r}_2^{CG} \times \boldsymbol{T} + \boldsymbol{\tau}, \tag{2}$$

where $\boldsymbol{x} \in \mathbb{R}^3$ is position, $m \in \mathbb{R}$ is the total mass of the vehicle, $g \in \mathbb{R}$ is the gravitational constant, $J \in \mathbb{R}^{3\times3}$ is the inertia tensor resolved on O_1 with a displaced origin coincident to the system's center of gravity (CG), $\boldsymbol{\omega} \in \mathbb{R}^3$ is the angular velocity resolved at O_1, $\boldsymbol{\tau} \in \mathbb{R}^3$ is the reaction torque caused by the rotors and the control surfaces, and $\boldsymbol{r}_2^{CG} \in \mathbb{R}^3$ is the vector from CG to O_2, where $\boldsymbol{T}$ is applied. Furthermore, here we assume that the control vanes cause the resultant thrust vector $\boldsymbol{T}$ to tilt perpendicularly to the core's DoF.

B. FLIGHT CONTROL

Because the system is underactuated, the position control uses a cascade structure, as shown in Fig. 7. The control scheme used here is based on that used for unidirectional multirotor UAVs [36], [37]. The outer position control loop is a self-contained cascade, with a proportional controller for position and a PID controller for velocity. The desired force $\boldsymbol{T}_{dp} \in \mathbb{R}^3$ is the main output expressed in the inertial reference frame. The control law is defined as

$$\begin{aligned}\boldsymbol{T}_{dp} = {} & \mathbf{K}_p(\boldsymbol{x}_d - \boldsymbol{x}) + \mathbf{K}_{dp}(\dot{\boldsymbol{x}}_d - \dot{\boldsymbol{x}}) + \mathbf{K}_{dd}(\ddot{\boldsymbol{x}}_d - \ddot{\boldsymbol{x}}) \\ & + \mathbf{K}_{di}\int(\dot{\boldsymbol{x}}_d - \dot{\boldsymbol{x}})dt - m\,g\,\hat{\boldsymbol{z}},\end{aligned} \tag{3}$$

where $\mathbf{K}_p$, $\mathbf{K}_{dp}$, $\mathbf{K}_{dd}$, $\mathbf{K}_{di} \in \mathbb{R}^{3\times3}$ are positive definite diagonal gain matrices, and $\boldsymbol{x}_d \in \mathbb{R}^3$ is the desired position. The calculated thrust direction is then fed to the attitude controller, which is also divided into two cascaded loops. The outer loop is based on quaternion error, where the desired attitude is a unit quaternion $\hat{\boldsymbol{q}}_d \in \mathbb{S}^3$. To achieve stability, the desired attitude is defined as

$$\hat{\boldsymbol{z}}_d = -\frac{\boldsymbol{T}_{dp}}{\|\boldsymbol{T}_{dp}\|}, \tag{4}$$

and the quaternion error, $\boldsymbol{q}_e \in \mathbb{S}^3$, is determined by the quaternion product

$$\boldsymbol{q}_e = \hat{\boldsymbol{q}}^{-1}\,\hat{\boldsymbol{q}}_d, \tag{5}$$

representing the rotation from $\hat{\boldsymbol{q}}$ to $\hat{\boldsymbol{q}}_d$. Given the defined error, the attitude controller control law then becomes

$$\boldsymbol{\omega}_d = k_r\,sign(\boldsymbol{q}_{e,0})\,\boldsymbol{q}_{e,1:3}, \tag{6}$$

where $\boldsymbol{\omega}_d \in \mathbb{R}^3$ is the desired angular velocity, $k_r \in \mathbb{R}$ is a tuning gain, and $sign(\,)$ is a function that outputs the sign, positive or negative, of its input. Finally, the control law for the rate controller is

$$\boldsymbol{\tau}_d = \mathbf{K}_\omega\,(\boldsymbol{\omega}_d - \boldsymbol{\omega}) + \boldsymbol{\omega} \times J\,\boldsymbol{\omega}, \tag{7}$$

where $\mathbf{K}_\omega \in \mathbb{R}^{3\times3}$ is a gain matrix, and $\boldsymbol{\tau}_d \in \mathbb{R}^3$ is the desired torque to control attitude.

C. CONTROL OF THE VANES

As previously stated, while the vehicle hovers, its CG is aligned with the kinematic singularity of the gimbal. We keep the initial DoF fixed to control the UAV at this operating pose, and the vanes movement coordination compensates on the pitch axis. It is vital to notice that the vanes are not controlled by a model. In contrast to the well-known and researched rotors typically used on multirotor UAVs, the authors could not find any study in the literature that describes a system similar to the one employed here, i.e., a counter-rotating coaxial rotor system with control surfaces positioned in between them. Because the interaction between the vanes and the rotors is undoubtedly complicated, and a discussion of such a system would be beyond the scope of this paper, we do not attempt to model the system here, leaving it for future work. As a result, implementation-wise, the vanes are controlled by a correctly adjusted flight controller mixer. Given that the vanes are controlled independently by separate servos, we assume that they might contribute to system regulation in two ways: i) help to control rotations about $\hat{z}_b$, or yaw, and ii) control the vehicle's pitch or rotations about $\hat{y}_b$. To exert moment about $\hat{z}_b$, the mixer commands the vanes to move deferentially with regard to $\hat{z}_b$ (Fig. 8 a)). To control pitch (rotations about $\hat{y}_b$), the mixer commands the vanes to rotate symmetrically about $\hat{y}_b$ (Fig. 8 b)). Mathematically, the mixer controlling the vanes is expressed as

$$\alpha_1 = k_{yaw}\,\tau_{dz} + k_{pitch}\,\tau_{dy}, \tag{8}$$

$$\alpha_2 = k_{yaw}\,\tau_{dz} - k_{pitch}\,\tau_{dy}, \tag{9}$$

where $\tau_{dy} \in \mathbb{R}$ and $\tau_{dz} \in \mathbb{R}$ are the y and z components of τ_d, $k_{yaw} \in \mathbb{R}$ and $k_{pitch} \in \mathbb{R}$ are gains, and α_1 refers to the vane

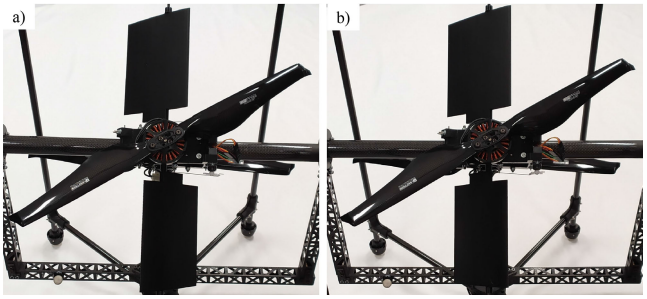

FIGURE 8. The configurations that the vanes can attain to contribute to the control of the Omnirotor's attitude. a) Generic pose to control yaw, rotation about $\hat{z}_b$, and b) generic pose for controlling pitch, rotation about $\hat{y}_b$.

mounted on the positive side of $\hat{y}_2$, and α_2 refers to the vane mounted on the negative side of $\hat{y}_2$.

V. EXPERIMENTAL RESULTS AND DISCUSSIONS

In this section, we present the main experimental results of the work together with the specific control methods that are used in each of the Omnirotor all-terrain platform's operation modes and configurations. Fig. 9 shows a tree-like schematic that summarizes the five operation configurations of the Omnirotor and their connections to the two different operation modes. As mentioned, the Omnirotor can operate in two fundamentally different modes, flight mode, and ground mode. The combination of the continuous omnidirectional thrust vectoring ability and the positions of the vehicle's CG and rotors shown in Fig. 4 facilitates the implementation of operational configurations that branch out from the two modes. The flight mode consists of two operational configurations, as the platform can fly in both the Inverted and the Normal equilibrium configuration. The ground mode consists of two operational configurations, as the platform can drive on the ground in both the Inverted and the Normal configurations. Finally, the platform also has a recovery process that can restore the vehicle from any non-operational configuration (sideways landing) into the Normal operating configuration.

A. INVERTED FLIGHT CONFIGURATION

The attitude control outputs the desired torque applied to the vehicle's CG, which must still be converted into the forces our design can exert, namely the rotor thrust and the forces generated by the control vanes deflection. For thrust only, the forward mapping is the cross product between $\boldsymbol{r}_2^{CG}$ and $\boldsymbol{T}$, as in the right-hand side of eq. (2). Therefore, it is reasonable to have the inverse map defined simply as

$$\boldsymbol{T}_{d\tau} = [\boldsymbol{r}_2^{CG}\times]^{\dagger}\,\boldsymbol{\tau}_d, \tag{10}$$

where $[\boldsymbol{r}_2^{CG}\times]^{\dagger} \in \mathbb{R}^{3\times 3}$ is the Moore-Penrose pseudo-inverse of the skew-symmetric matrix representation of the cross-product of $\boldsymbol{r}_2^{CG}$. Finally, the total force the rotor on the gimbal has to exert, $\boldsymbol{T}_d \in \mathbb{R}^3$, is defined as

$$\boldsymbol{T}_d = \boldsymbol{T}_{d\tau} + \left(\boldsymbol{T}_{dp}\,.\,\hat{z}_b\right)\hat{z}_b, \tag{11}$$

where [.] indicates the dot product.

Given the total desired force, now inverse kinematics is needed to track such forces. This flight configuration has been demonstrated in [6] with the previous version of the concept. However, this version has the flight controller placed on the Fork body (frame O_1), instead of on the Cage body (frame B). Therefore, the inverse kinematics is simplified. When flying, the first DoF of the gimbal mechanism is not used and is kept locked in position. For the control of the second DoF in the gimbal, the desired angle with respect to $\hat{z}_1$ is defined as

$$\theta_2 = atan2\left(\hat{\boldsymbol{T}}_d\,.\,\hat{\boldsymbol{x}}_1\ ,\ \hat{\boldsymbol{T}}_d\,.\,\hat{z}_2\right) \tag{12}$$

Please note that $\hat{\boldsymbol{T}}_d\,.\,\hat{\boldsymbol{x}}_1$ and $\hat{\boldsymbol{T}}_d\,.\,\hat{z}_2$ are just the x and z component of the normalized $\boldsymbol{T}_d$ vector when expressed in O_1, respectively. The function $atan2()$ produces only one point of convergence, forcing the solution to converge to a specific configuration that coincides with the desired thrust' derived from eq. (11).

B. NORMAL FLIGHT CONFIGURATION

The flight control of the Omnirotor in the Normal flight configuration is not very different from the Inverted one. The versatility of the design enables the vehicle to use the same basic underlying attitude controller, with the difference that the desired attitude for hovering is rotated 180° about the second DoF's axis. Since in this configuration, the Core body's frame is no longer aligned with the other frames, in order to keep the commands to the actuators consistent, roll and yaw output torques are negated, as well as the z component of $\boldsymbol{T}_d$. The changes can be summarized by

$$\hat{\boldsymbol{q}}_{d\,new} = \hat{\boldsymbol{q}}_r(\pi, 0, 0)\,\hat{\boldsymbol{q}}_d, \tag{13}$$

$$\boldsymbol{\tau}_d\,.\,\hat{\boldsymbol{x}}_1 = -\,\boldsymbol{\tau}_d\,.\,\hat{\boldsymbol{x}}_1, \quad \boldsymbol{\tau}_d\,.\,\hat{z}_1 = -\,\boldsymbol{\tau}_d\,.\,\hat{z}_1,$$

$$\textit{and} \quad \boldsymbol{T}_d\,.\,\hat{z}_1 = -\,\boldsymbol{T}_d\,.\,\hat{z}_1. \tag{14}$$

In the above equation, all quantities refer to the O_1 frame. Output torques for pitch ($\boldsymbol{y}_1$) are an exception because the resulting orientation of such axis after a 180° rotation about the $\boldsymbol{x}_1$ already causes the effect of negating the relationship between rotation about that axis and the desired response of the vanes to control pitch.

C. INVERTED AND NORMAL FLIGHT CONFIGURATIONS VS TAKEOFF

The Omnirotor behaves quite differently in the Inverted configuration than in the Normal one. For the Inverted orientation, because the center of mass is above the rotors and the Omnirotor is based on tilt-rotor propulsion, if, for example, it wants to generate a torque tilting the vehicle to the right, it needs first to point the rotor to the left. Systems with such characteristics are denoted as non-minimum phase systems, which examples include the Inverted pendulum on

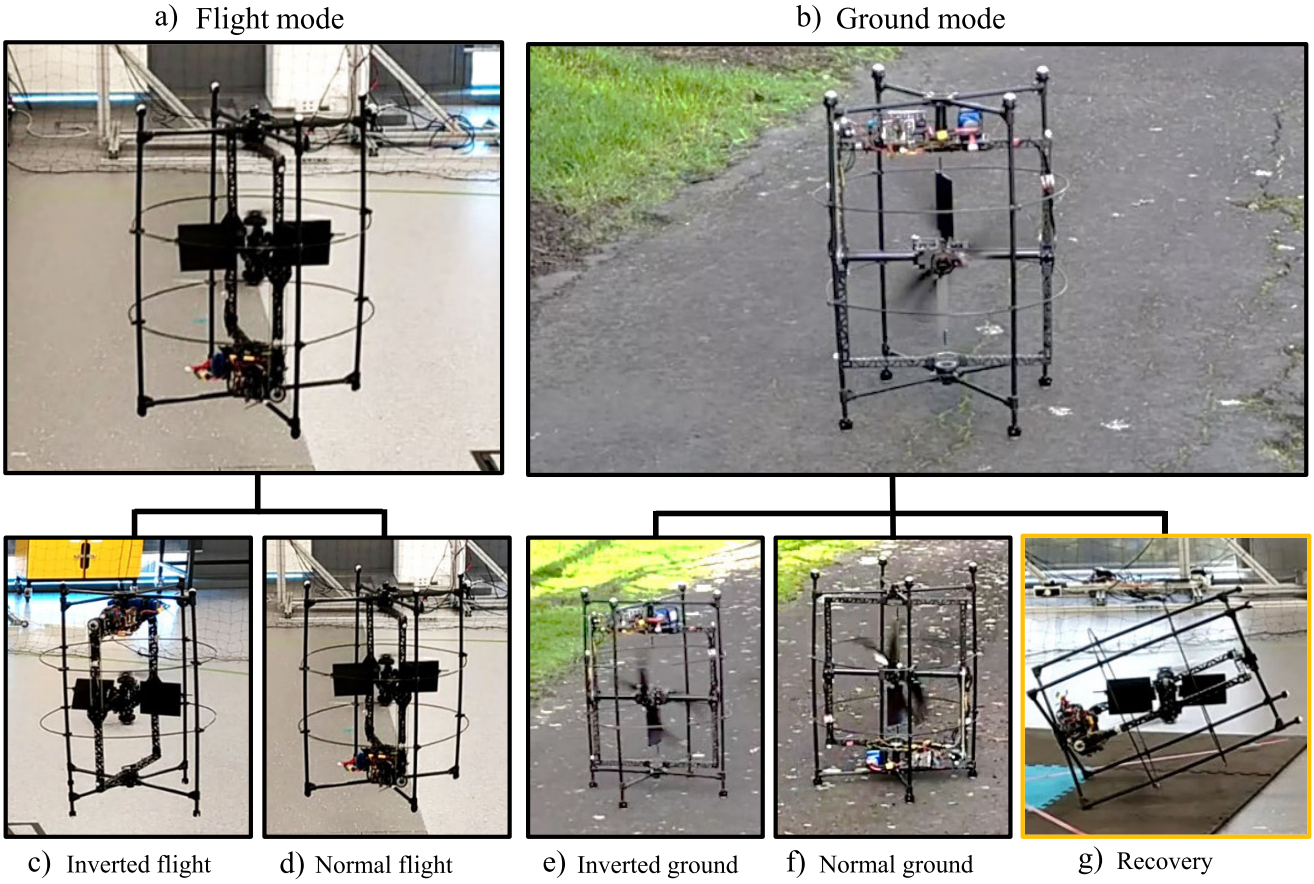

FIGURE 9. Schematic illustrating the Omnirotor's modes of operation and their respective operation configurations. The concept has two operating modes, a) flight mode, when it works as an aerial vehicle, and b) ground mode, when it works as a ground vehicle. The flight mode has two operation configurations, given it can fly in two different poses we denote as c) Inverted and d) Normal. While on the ground, the vehicle can operate in three different configurations. It can drive on the ground in the e) Inverted pose, and f) Normal pose, and it can also restore its orientation to the Normal ground pose with its g) recovery process. This last functionality is highlighted in yellow in the image to distinguish it as a process that transitions the vehicle from any non-operational configuration to the Normal or Inverted configuration.

a cart problem [38], attitude control problem for fixed wings aircrafts [39], and rockets or missiles [40], [41]. This characteristic becomes especially important during takeoff, where the vehicle is in contact with the ground at the start and can behave differently. When laying on a flat, smooth surface, a slow takeoff on the Inverted pose can lead the vehicle to slide on the ground, gaining speed in the opposite direction it would go if it was hovering in the air. However, if the surface is inclined, this is bound to happen, as the controller tries to compensate for the tilting of the vehicle from the beginning.

In a worst-case scenario, the vehicle would be taking off from an inclined, rough surface that does not allow sliding. An example of this case would be a grassy hill. A series of experimental results obtained in such conditions and outdoor environments (a public park) are shown in Figure 10. In this experiment, the grassy hill has an inclination of approximately 9°, and a trained pilot using the radio controller performs the takeoff. The images and plots show the time instances of the vehicle attempting to takeoff from the Inverted pose and finally the vehicle flipping due to the grass to a sideways non-operational configuration. As expected, the non-minimal phase characteristics of the vehicle led to failure from taking off. From the beginning, the rotors are pointed towards the inclination direction of the vehicle. As thrust increases, the vehicle starts to tilt even more towards the lower side of the hill, and the controller tries to compensate for this by further tilting the rotors in the same direction. This self-feeding behavior eventually leads the robot to fall on its side and attain a non-operational configuration.

On the other hand, the Normal flight attitude does not possess the non-minimal phase characteristics, making it a much better option when the vehicle needs to takeoff from difficult terrain. This is further supported by the results presented in Figure 11. In such experiments, the vehicle was placed on the same hill but now in the Normal configuration. From the start, in e), the rotors are now pointed in the upwards direction of the hill in a way that appropriately compensates the inclination of the vehicle even when in contact with the ground. In the following images, the vehicle corrects its attitude, takeoff, and starts flying. From the plots, it is noticeable that the robot has a low-frequency oscillation due to starting from an inclined surface. Despite the advantage

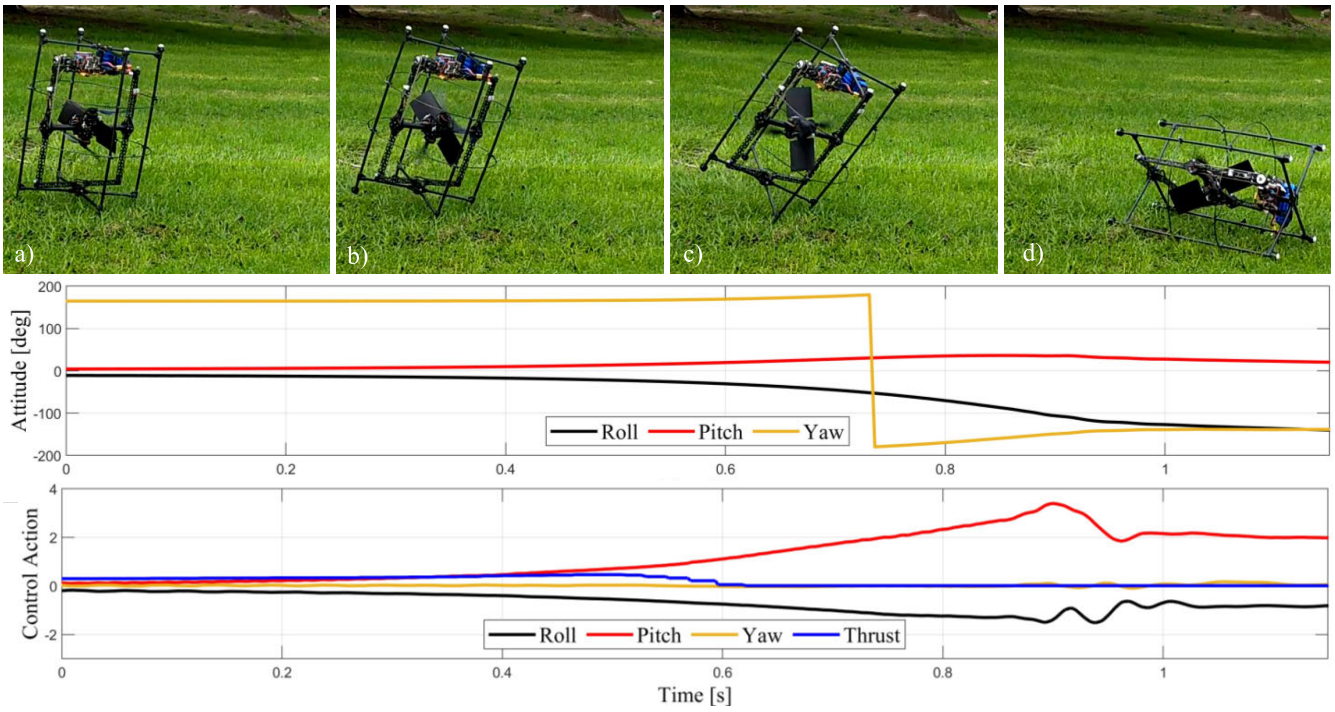

FIGURE 10. Worst case scenario example showing the behavior of the Inverted flight configuration when taking off from inclined surfaces that also restrict sliding. Given its non-minimum phase behavior, the constraint imposed by the grass that restricts sliding, together with the need to compensate for the attitude error caused by the inclination, the vehicle fails to takeoff flipping on the side. From a) to d), it can be noted that the larger the inclination of the vehicle, the larger the angle of the rotors. This self-feeding behavior is also very clear from the accompanying plots showing the control action and the vehicle's attitude over time.

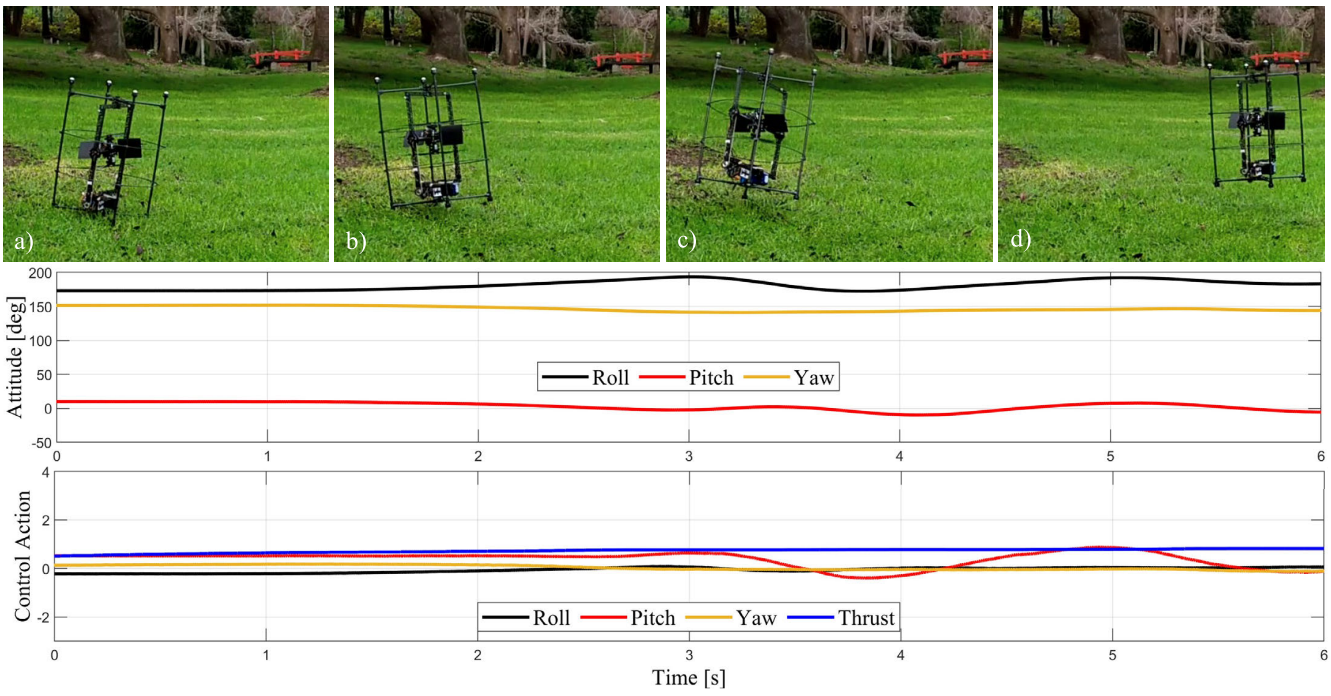

FIGURE 11. Differently from the Inverted flight configuration, the Normal flight configuration lacks the non-minimum phase behavior and, therefore, can takeoff from the inclined surface with no problem. In a) and b), it is possible to observe that the vehicle correctly orients itself by directing the rotors' thrust to a direction that favors stability and that taking off from the inclined surface only has the effect of inducing an initial oscillation to the vehicle's attitude, as shown by c), d), and the accompanying plots.

of having minimal phase, the Normal flight mode suffers from having lower flight efficiency. When flying in this mode, the battery and electronics sit right below the rotors, shadowing the propeller's slipstream, reducing thrust capacity and, consequently, efficiency. The Omnirotor's efficiency when flying in the Inverted configuration is 5.14 g/W versus

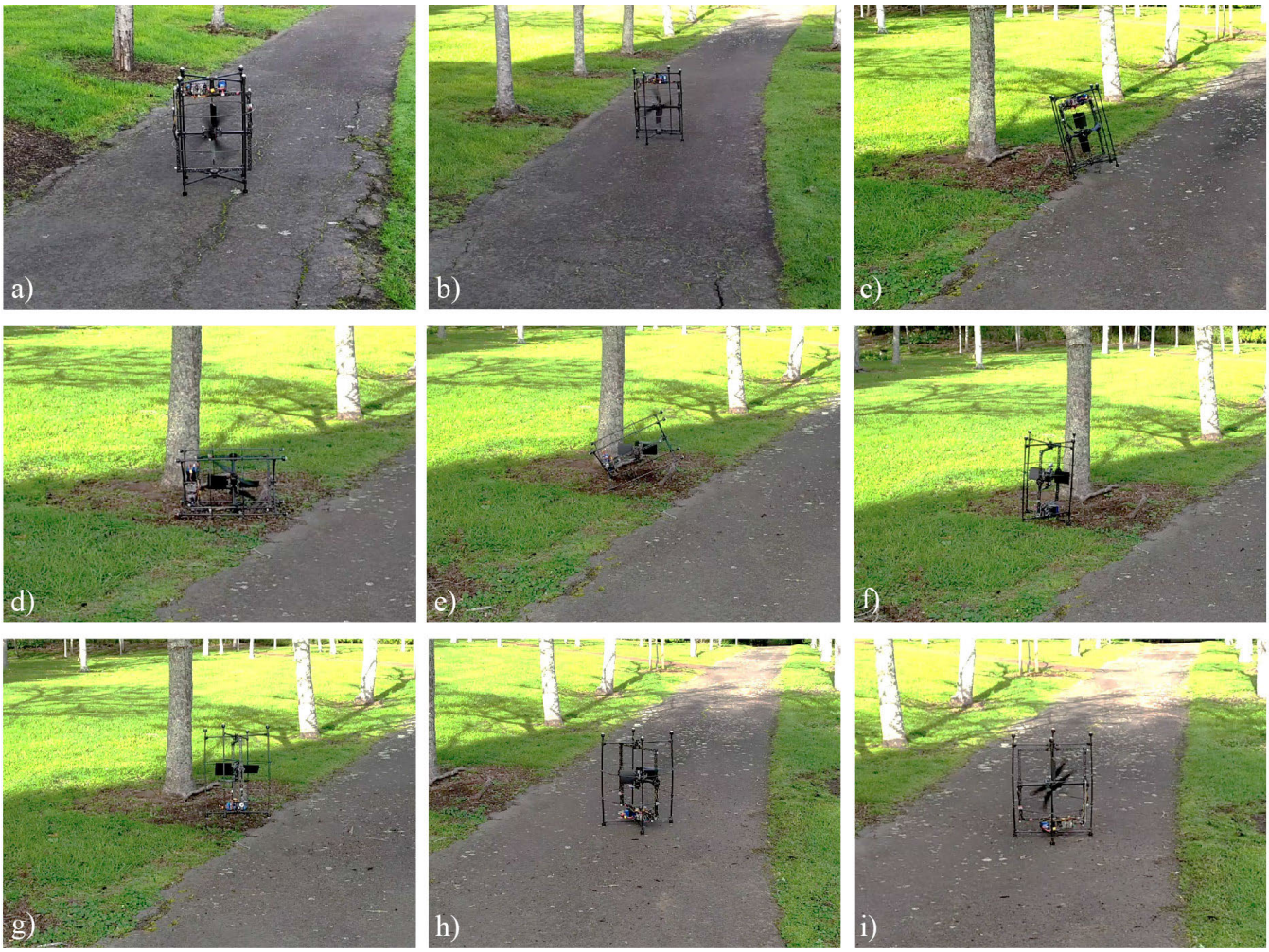

FIGURE 12. Recovery process demonstration in a public park experiment simulating a field mission. In a) and b), the vehicle is operating in ground mode, driving along a paved pathway; in c), it experiences an unexpected event that causes it to get off the path and hit the grass; and in d), tilt and fall on its side. The pilot changes the vehicle to operate using the recovery process. The rotors are now pointing upwards, tracking the direction of gravity; in e) with enough throttle, the robot starts to correct itself, and in f) it lands on the Normal orientation, after which it can then change to flight mode in the Normal configuration, and g) takeoff and fly very shortly back spending a minimum amount of energy, finally in h) it lands on the pathway. In I), the pilot changes the Omnirotor back to the ground mode in the Normal configuration and resumes the mission controlling the vehicle as a ground robot.

4.46 g/W when flying in the Normal configuration, making flying Inverted 15.2% more efficient than flying in the Normal configuration. This difference indicates that the Normal flight configuration is more useful for taking-off off inclined surfaces and flights of short duration. For long flights, flying Inverted is more advantageous.

D. GROUND RECOVERY PROCESS

Another advantage of having the vehicle based on the continuous omnidirectional thrust vectoring concept is that it can use such omnidirectionality to self-recover after a crash. Suppose the Omnirotor falls in any orientation other than the operational configurations. In that case, the rotor-on-gimbal mechanism can use the sensor data from the flight controller to redirect thrust and track the direction of gravity. This can be considered as a vehicle operation process of the ground mode, called 'Recovery.' In this process, the attitude controller outputs are ignored, and the vehicle responds only to the orientation of gravity and the pilot's throttle input. The kinematics is described by

$$\theta_1 = atan\left(\frac{\hat{\boldsymbol{g}} \,.\, \hat{\boldsymbol{x}}_1}{\hat{\boldsymbol{g}} \,.\, \hat{\boldsymbol{y}}_1}\right), \tag{15}$$

$$\theta_2 = atan2\left(\hat{\boldsymbol{g}} \,.\, \hat{\boldsymbol{y}}_1 \;,\; \hat{\boldsymbol{g}} \,.\, \hat{\boldsymbol{z}}_1\right), \tag{16}$$

where $\hat{\boldsymbol{g}}$ is the normalized gravity vector expressed on O_1. The process is used to bring the vehicle from a random non-operational orientation to its most stable configuration when no attitude controller is involved, which is the Normal orientation. When the robot is allowed to rotate, as in the case of no attitude controller, the Normal pose is the natural orientation for it simply because the CG has lower potential energy in that pose, meaning that it is closer to the ground (see Fig. 4). This is an important differentiation between the two drive modes of the vehicle. When Inverted, it can switch

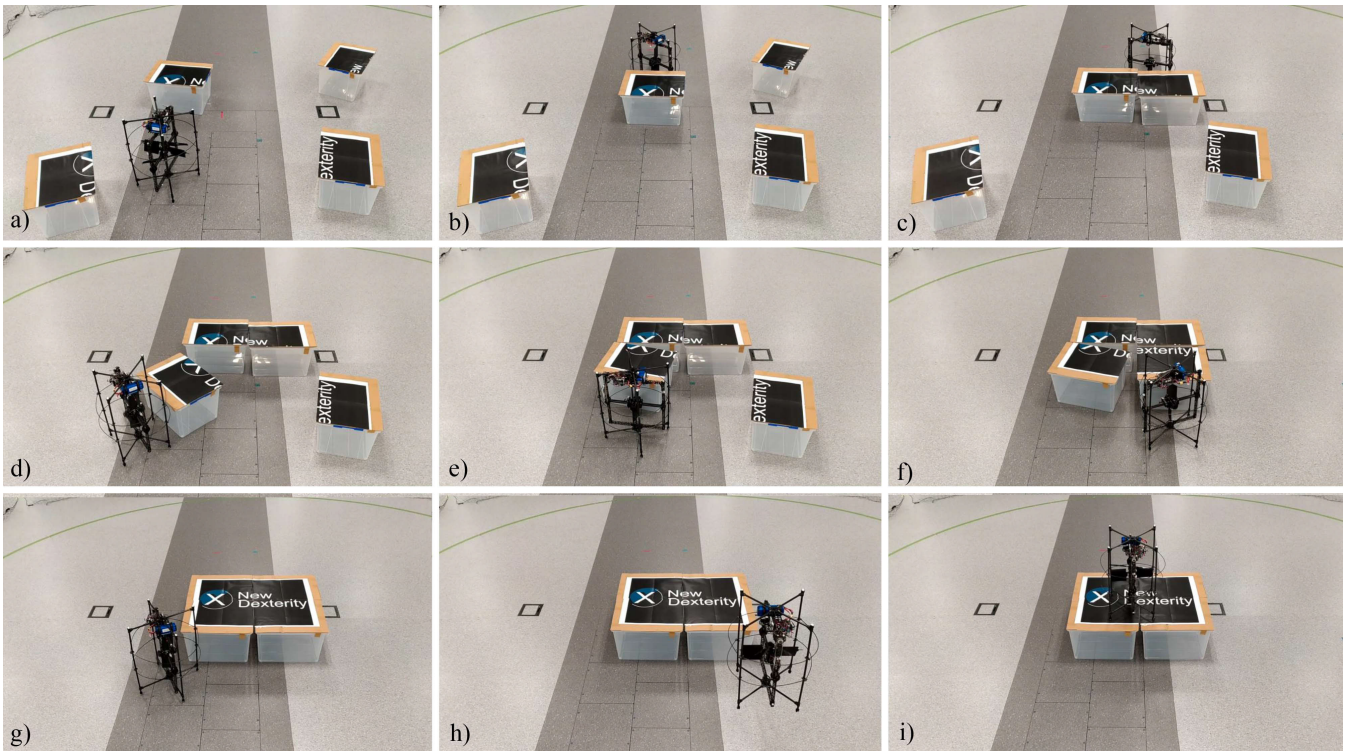

FIGURE 13. Demonstration of how the full-thrust availability of the vehicle in ground mode can be used for interaction and ground push-based manipulation of objects. In this experiment, a puzzle composed of four boxes with matched tiles is assembled by the Omnirotor. In a), the four boxes are spread randomly throughout the room. Teleoperating the device, the pilot controls the vehicle to push the boxes on the ground and assemble the puzzle. Note that through b), c), d), e), and f), not only the position of the boxes must be changed, but also their orientation on the ground. The assembly of the full puzzle took about 10 minutes and, although time-consuming, was not a hard task for the pilot, being completed with no problems on the first try. This is partially thanks to the holonomic characteristics of the Omnirotor in ground mode, which allows for considerable precise maneuvering of the box, enough to finish the puzzle with no significant gaps in the image formed by the boxes as seen in g). Furthermore, the boxes also provide an elevated platform, on which the vehicle can takeoff as seen in h) and land on it as seen in i).

to Normal. However, once in Normal, it can not switch back to Inverted, which provides more efficient flying.

In Figure 12, we demonstrate a scenario where the recovery process is used to restore the vehicle to its Normal operational state after flipping on a non-operational configuration during a simulated field mission. At the beginning of the mission, the Omnirotor is operating in ground mode, surveying a park by driving along the paved paths. During an unexpected eventuality, such as a strong wind gust or the need to give away space for passers-by to cross the pathway, the robot is forced out of the path and trips on the grass, causing it to tilt and fall on its side. The operator then changes the vehicle to the recovery process option, and it starts pointing the rotors up in the direction of gravity e), regardless of the vehicle's current orientation. The pilot only has to provide a throttle, causing the vehicle to tilt and eventually land on the Normal pose. Once in this stable pose, the vehicle switches to the Normal flight configuration and can takeoff and fly for a short period only to exit the unsuitable terrain and return to the pathway, saving as much energy as possible. In the pathway, it can switch back to the ground mode, which works both in the Inverted and Normal configuration, and resume the mission, driving along the pathway as a mobile robot.

E. GROUND MODE AND PUSH-BASED MANIPULATION

To operate as a ground robot, the Omnirotor has to simply redirect the rotors to apply thrust horizontally and point it in the direction it wants to move. Albeit simple and without the need for a controller to stabilize the vehicle, the ground mode of operation of the Omnirotor provides many possibilities. The first is that it makes the vehicle hybrid, capable of operating as both a UGV and a UAV. In this sense, the main advantage of operating in ground mode is saving energy and increasing vehicle autonomy. Even when driving on rough terrain and uphill, such as in Figure 12, the vehicle requires only about 25% of throttle to move, which consumes about 115 W of power. This decreases dramatically the amount of energy consumed during operation when compared to hovering, which requires about 75% of throttle in the Inverted configuration and consumes 720 W of power. In turn, such difference is reflected in operational time, as shown in Table 2. Note also that, on smooth flat surfaces, the required throttle to move falls below 15%, which should increase even further the platform's autonomy.

A particular advantage of the ground operation mode of the Omnirotor is that it is holonomic, meaning it can move in any direction regardless of its current pose. This is a

direct consequence of the concept's continuous omnidirectional thrust vectoring ability and of the choice of caster wheels in the design, which is based on a ball rolling on a socket and, therefore, also holonomic. However, during the ground mode, the vehicle has no control over the orientation of the cage, which is left to rotate freely. Together with the fact that the entire thrust of the rotors can be directed horizontally, the holonomic characteristics of the ground mode enable the Omnirotor to perform complex and demanding tasks such as push-based manipulation of objects on the ground.

The experiment shown in Figure 13 was designed to illustrate the manipulation capabilities of the Omnirotor while in ground mode. It consists of a puzzle made of four boxes with matching tiles. In the beginning, the boxes are spread randomly on the floor, as in Figure 13 a). The goal is to bring the boxes together in a matching way to form the image, and this is performed by a pilot remote-controlling the Omnirotor. It is interesting to note that, while time-consuming, as the whole assembly took about 10 minutes, it was not hard from the pilot's perspective and was done in a single try and with good enough precision to leave no gaps in the final image assembly.

Many factors contribute to the resulting low level of difficulty in executing the task. One of them is the holonomic nature of the ground mode, which allows for changing the moving direction at any time. As the Omnirotor's cage shape resembles a cylinder when pushing on something, the interaction is similar to a line contact, where only a force is applied. The moment from the line does not influence the orientation of the box on the plane. Therefore, if the contact point is aligned with the CG of the box, then only translation happens. If the contact point is not aligned, then there will be a coupled rotation and translation of the box. By changing the contact point, the pilot can control how to move the box, both its position and orientation.

Finally, the end result of the assembled puzzle also forms a platform above the ground, suitable for the vehicle to land on, as demonstrated in Figure 13 h) and i). This is just an example, but it can illustrate how such a hybrid UAV/UGV vehicle with effective ground manipulation capabilities can be used to modify its environment and to help with the assembly and construction of structures. We believe that there are many scenarios where the Omnirotor can be useful. For example, in search-and-rescue scenarios with collaboration between different robots, where the Omnirotor could remove debris and clear a path for another robot with no manipulation capabilities to pass, such as pushing open a door or a chair or rearranging structures to build a path like platforms and ramps.

F. VIDEO DEMONSTRATION

An HD-quality video demonstration of the proposed device and the open-source code used in the platform can be found at the following url: www.newdexterity.org/Omnirotor

VI. CONCLUSION

This paper presented the New Dexterity Omnirotor platform, which is a hybrid, multi-modal UAV/UGV hybrid, all-terrain vehicle capable of continuous omnidirectional thrust vectoring. The vehicle concept has two distinct operational modes, flight, and ground, where it can work as both an aerial and a ground vehicle, respectively. Additionally, it has a total of five operational configurations that are derived from the two operation modes. In flight mode, it can fly in two configurations, Normal and Inverted, with Inverted being 15% more efficient. In ground mode, it can work in three configurations, driving on the ground in both the Inverted and Normal configurations, and recovering from non-operational configurations. In particular, the recovery process can bring the vehicle from any non-operational state to the Normal ground configuration, where it can either fly or drive on the ground. However, recovery to the Inverted state is currently not possible. This paper presented in detail the concept and design of the Omnirotor vehicle that enables continuous omnidirectional thrust vectoring. Furthermore, it also presented the modeling and control used for the presented modes and configurations, all of which were demonstrated in experiments that involved multiple modes and configurations working together to transverse challenging environments, such as a park. Additionally, beyond the locomotion configurations, the Omnirotor is capable of performing ground push-based manipulation of objects. Such skills are demonstrated in a puzzle experiment where matching boxes are assembled to build a landing platform for the vehicle. Future directions for the concept will include its use in a swarm of robots that exhibits both ground and aerial manipulation capabilities.

REFERENCES

[1] D. Mellinger, Q. Lindsey, M. Shomin, and V. Kumar, "Design, modeling, estimation and control for aerial grasping and manipulation," in *Proc. IEEE/RSJ Int. Conf. Intell. Robot. Syst. (IROS)*, Sep. 2011, pp. 2668–2673.

[2] P. E. I. Pounds, D. R. Bersak, and A. M. Dollár, "Grasping from the air: Hovering capture and load stability," in *Proc. IEEE Int. Conf. Robot. Autom. (ICRA)*, May 2011, pp. 2491–2498.

[3] A. Kalantari and M. Spenko, "Design and experimental validation of HyTAQ, a hybrid terrestrial and aerial quadrotor," in *Proc. IEEE Int. Conf. Robot. Autom.*, May 2013, pp. 4445–4450.

[4] S. Latscha, M. Kofron, A. Stroffolino, L. Davis, G. Merritt, M. Piccoli, and M. Yim, "Design of a hybrid exploration robot for air and land deployment (H.E.R.A.L.D) for urban search and rescue applications," in *Proc. IEEE/RSJ Int. Conf. Intell. Robots Syst.*, Sep. 2014, pp. 1868–1873.

[5] J. Buzzatto and M. Liarokapis, "An agile, coaxial, omnidirectional rotor module: On the development of hybrid, all terrain robotic rotorcrafts," in *Proc. IEEE Int. Symp. Saf., Secur., Rescue Robot. (SSRR)*, Nov. 2020, pp. 162–168.

[6] J. Buzzatto, P. H. Mendes, N. Perera, K. Stol, and M. Liarokapis, "The new dexterity omnirotor platform: Design, modeling, and control of a modular, versatile, all-terrain vehicle," in *Proc. IEEE/RSJ Int. Conf. Intell. Robots Syst. (IROS)*, Sep. 2021, pp. 6336–6343.

[7] J. Buzzatto and M. Liarokapis, "A benchmarking platform and a control allocation method for improving the efficiency of coaxial rotor systems," *IEEE Robot. Autom. Lett.*, vol. 7, no. 2, pp. 5302–5309, Apr. 2022.

[8] H. B. Khamseh, F. Janabi-Sharifi, and A. Abdessameud, "Aerial manipulation—A literature survey," *Robot. Auto. Syst.*, vol. 107, pp. 221–235, Sep. 2018.

[9] J. Meng, J. Buzzatto, Y. Liu, and M. Liarokapis, "On aerial robots with grasping and perching capabilities: A comprehensive review," *Frontiers Robot. AI*, vol. 8, p. 405, Mar. 2022.

[10] K. Kondak, F. Huber, M. Schwarzbach, M. Laiacker, D. Sommer, M. Bejar, and A. Ollero, "Aerial manipulation robot composed of an autonomous helicopter and a 7 degrees of freedom industrial manipulator," in *Proc. IEEE Int. Conf. Robot. Autom. (ICRA)*, May 2014, pp. 2107–2112.

[11] K. Steich, M. Kamel, P. Beardsley, M. K. Obrist, R. Siegwart, and T. Lachat, "Tree cavity inspection using aerial robots," in *Proc. IEEE/RSJ Int. Conf. Intell. Robots Syst. (IROS)*, Oct. 2016, pp. 4856–4862.

[12] A. Q. L. Keemink, M. Fumagalli, S. Stramigioli, and R. Carloni, "Mechanical design of a manipulation system for unmanned aerial vehicles," in *Proc. IEEE Int. Conf. Robot. Autom.*, May 2012, pp. 3147–3152.

[13] (2020). *WingtraOne VTOL Fixed-Wing UAV*. [Online]. Available: https://wingtra.com/

[14] B. Coxworth. (2019). *DHL Parcelcopter Takes to Tanzanian Skies*. [Online]. Available: https://newatlas.com/dhl-parcelcopter-africa/56663/

[15] J. L. J. Scholten, M. Fumagalli, S. Stramigioli, and R. Carloni, "Interaction control of an UAV endowed with a manipulator," in *Proc. IEEE Int. Conf. Robot. Autom.*, May 2013, pp. 4910–4915.

[16] S. Kim, H. Seo, and H. J. Kim, "Operating an unknown drawer using an aerial manipulator," in *Proc. IEEE Int. Conf. Robot. Autom. (ICRA)*, May 2015, pp. 5503–5508.

[17] H. W. Wopereis, J. J. Hoekstra, T. H. Post, G. A. Folkertsma, S. Stramigioli, and M. Fumagalli, "Application of substantial and sustained force to vertical surfaces using a quadrotor," in *Proc. IEEE Int. Conf. Robot. Autom. (ICRA)*, May 2017, pp. 2704–2709.

[18] M. Ryll, G. Muscio, F. Pierri, E. Cataldi, G. Antonelli, F. Caccavale, and A. Franchi, "6D physical interaction with a fully actuated aerial robot," in *Proc. IEEE Int. Conf. Robot. Autom. (ICRA)*, May 2017, pp. 5190–5195.

[19] C. Papachristos, K. Alexis, and A. Tzes, "Efficient force exertion for aerial robotic manipulation: Exploiting the thrust-vectoring authority of a tri-tiltrotor UAV," in *Proc. IEEE Int. Conf. Robot. Autom. (ICRA)*, May 2014, pp. 4500–4505.

[20] M. Kamel, S. Verling, O. Elkhatib, C. Sprecher, P. Wulkop, Z. Taylor, R. Siegwart, and I. Gilitschenski, "The voliro omniorientational hexacopter: An agile and maneuverable tiltable-rotor aerial vehicle," *IEEE Robot. Autom. Mag.*, vol. 25, no. 4, pp. 34–44, Dec. 2018.

[21] P. Zheng, X. Tan, B. B. Kocer, E. Yang, and M. Kovac, "TiltDrone: A fully-actuated tilting quadrotor platform," *IEEE Robot. Autom. Lett.*, vol. 5, no. 4, pp. 6845–6852, Oct. 2020.

[22] Y. Qin, W. Xu, A. Lee, and F. Zhang, "Gemini: A compact yet efficient bi-copter UAV for indoor applications," *IEEE Robot. Automat. Lett.*, vol. 5, no. 2, pp. 3213–3220, Apr. 2020.

[23] J. R. Page and P. E. I. Pounds, "The quadroller: Modeling of a UAV/UGV hybrid quadrotor," in *Proc. IEEE/RSJ Int. Conf. Intell. Robots Syst.*, Sep. 2014, pp. 4834–4841.

[24] D. D. Fan, R. Thakker, T. Bartlett, M. B. Miled, L. Kim, E. Theodorou, and A.-A. Agha-Mohammadi, "Autonomous hybrid ground/aerial mobility in unknown environments," in *Proc. IEEE/RSJ Int. Conf. Intell. Robots Syst. (IROS)*, Nov. 2019, pp. 3070–3077.

[25] Y. Qin, Y. Li, X. Wei, and F. Zhang, "Hybrid aerial-ground locomotion with a single passive wheel," in *Proc. IEEE/RSJ Int. Conf. Intell. Robots Syst. (IROS)*, Oct. 2020, pp. 1371–1376.

[26] J. Yang, Y. Zhu, L. Zhang, Y. Dong, and Y. Ding, "SytaB: A class of smooth-transition hybrid terrestrial/aerial bicopters," *IEEE Robot. Autom. Lett.*, vol. 7, no. 4, pp. 9199–9206, Oct. 2022.

[27] C. J. Salaan, K. Tadakuma, Y. Okada, K. Ohno, and S. Tadokoro, "UAV with two passive rotating hemispherical shells and horizontal rotor for hammering inspection of infrastructure," in *Proc. IEEE/SICE Int. Symp. Syst. Integr. (SII)*, Dec. 2017, pp. 769–774.

[28] C. J. Salaan, K. Tadakuma, Y. Okada, Y. Sakai, K. Ohno, and S. Tadokoro, "Development and experimental validation of aerial vehicle with passive rotating shell on each rotor," *IEEE Robot. Autom. Lett.*, vol. 4, no. 3, pp. 2568–2575, Jul. 2019.

[29] S. Atay, M. Bryant, and G. Buckner, "The spherical rolling-flying vehicle: Dynamic modeling and control system design," *J. Mech. Robot.*, vol. 13, no. 5, Oct. 2021, Art. no. 050901.

[30] K. Tanaka, D. Zhang, S. Inoue, R. Kasai, H. Yokoyama, K. Shindo, K. Matsuhiro, S. Marumoto, H. Ishii, and A. Takanishi, "A design of a small mobile robot with a hybrid locomotion mechanism of wheels and multi-rotors," in *Proc. IEEE Int. Conf. Mechatronics Autom. (ICMA)*, Aug. 2017, pp. 1503–1508.

[31] A. Kalantari, T. Touma, L. Kim, R. Jitosho, K. Strickland, B. T. Lopez, and A.-A. Agha-Mohammadi, "Drivocopter: A concept hybrid aerial/ground vehicle for long-endurance mobility," in *Proc. IEEE Aerosp. Conf.*, Mar. 2020, pp. 1–10.

[32] J. Cacace, G. A. Fontanelli, and V. Lippiello, "A novel hybrid aerial-ground manipulator for pipeline inspection tasks," in *Proc. Aerial Robot. Syst. Phys. Interacting Environ. (AIRPHARO)*, Oct. 2021, pp. 1–6.

[33] A. Suarez, A. Caballero, A. Garofano, P. J. Sanchez-Cuevas, G. Heredia, and A. Ollero, "Aerial manipulator with rolling base for inspection of pipe arrays," *IEEE Access*, vol. 8, pp. 162516–162532, 2020.

[34] L. Daler, S. Mintchev, C. Stefanini, and D. Floreano, "A bioinspired multimodal flying and walking robot," *Bioinspiration Biomimetics*, vol. 10, no. 1, Jan. 2015, Art. no. 016005.

[35] K. Kim, P. Spieler, E.-S. Lupu, A. Ramezani, and S.-J. Chung, "A bipedal walking robot that can fly, slackline, and skateboard," *Sci. Robot.*, vol. 6, no. 59, Oct. 2021, Art. no. eabf8136.

[36] D. Brescianini, M. Hehn, and R. D'Andrea, "Nonlinear quadrocopter attitude control," ETH Zurich, Zürich, Switzerland, Tech. Rep., 2013, doi: 10.3929/ethz-a-009970340.

[37] L. Meier, D. Honegger, and M. Pollefeys, "PX4: A node-based multithreaded open source robotics framework for deeply embedded platforms," in *Proc. IEEE Int. Conf. Robot. Autom. (ICRA)*, May 2015, pp. 6235–6240.

[38] R. Gurumoorthy and S. R. Sanders, "Controlling non-minimum phase nonlinear systems–The inverted pendulum on a cart example," in *Proc. Amer. Control Conf.*, Jun. 1993, pp. 680–685.

[39] J. Hauser, S. Sastry, and G. Meyer, "Nonlinear control design for slightly non-minimum phase systems: Application to V/STOL aircraft," *Automatica*, vol. 28, no. 4, pp. 665–679, 1992.

[40] R. A. Nichols, R. T. Reichert, and W. J. Rugh, "Gain scheduling for H-infinity controllers: A flight control example," *IEEE Trans. Control Syst. Technol.*, vol. 1, no. 2, pp. 69–79, Jun. 1993.

[41] D. Chen and B. Paden, "Stable inversion of nonlinear non-minimum phase systems," *Int. J. Control*, vol. 64, no. 1, pp. 81–97, May 1996.

JOAO BUZZATTO (Graduate Student Member, IEEE) received the B.E. and M.Sc. degrees in mechanical engineering from the University of São Paulo, Brazil, in 2016 and 2019, respectively. He is currently pursuing the Ph.D. degree in mechatronics engineering with the New Dexterity Research Group, The University of Auckland, New Zealand. His research interests include developing novel drones and grippers for aerial grasping, search-and-rescue, interaction applications, including their design, modeling, and control, soft robotics, and dexterous manipulation.

MINAS LIAROKAPIS (Senior Member, IEEE) received the Diploma degree in computer engineering from the University of Patras, Patras, Greece, the M.Sc. degree in information technologies in medicine and biology from the National and Kapodistrian University of Athens, Athens, Greece, and the Ph.D. degree in mechanical engineering from the National Technical University of Athens, Athens. He is currently an Associate Professor with the Department of Mechanical and Mechatronics Engineering, The University of Auckland, New Zealand, and the Director of the New Dexterity Research Group (www.newdexterity.org). Previously, he was a Postdoctoral Associate with the GRAB Laboratory, Yale University, USA. He is also the Founder of OpenBionics initiative (www.openbionics.org) and a Co-Founder of OpenRobotHardware (www.openrobothardware.org) and HandCorpus (www.handcorpus.org). His research interests include providing robotics solutions to everyday life problems, modeling, designing, and controlling novel robotics and bionics hardware.